Published in final edited form as:
Biochemistry. 2008 January 15; 47(2): 627–639. doi:10.1021/bi701365e.

The flavodoxin from *Helicobacter pylori*: Structural Determinants of Thermostability and FMN Cofactor Binding

Nunilo Cremades[‡,§], **Adrián Velazquez-Campoy**[‡], **Ernesto Freire**[‖], and **Javier Sancho**[‡,§,*]

‡*Biocomputation and Complex Systems Physics Institute (BIFI). Facultad de Ciencias. Universidad de Zaragoza. 50009-Zaragoza, Spain*

§*Departamento de Bioquímica y Biología Molecular y Celular. Facultad de Ciencias. Universidad de Zaragoza. 50009-Zaragoza, Spain*

‖*Department of Biology. The Johns Hopkins University. Baltimore, Maryland 21218 US*

Abstract

Flavodoxin has been recently recognized as an essential protein for a number of pathogenic bacteria including *Helicobacter pylori*, where it has been proposed to constitute a target for antibacterial drug development. One way we are exploring to screen for novel inhibitory compounds is to perform thermal up-shift assays, for which a detailed knowledge of protein thermostability and cofactor binding properties is of great help. However, very little is known on the stability and ligand binding properties of *H. pylori* flavodoxin, and its peculiar FMN binding site together with the variety of behaviours observed within the flavodoxin family preclude extrapolations. We have thus performed a detailed experimental and computational analysis of the thermostability and cofactor binding energetics of *H. pylori* flavodoxin and we have found that the thermal unfolding equilibrium is more complex that any other previously described for flavodoxins as it involves the accumulation of two distinct equilibrium intermediates. Fortunately the entire stability and binding data can be satisfactorily fitted to a model, summarized in a simple phase diagram, where the cofactor only binds to the native state. On the other hand, we show how variability of thermal unfolding behaviour within the flavodoxin family can be predicted using structure-energetics relationships implemented in the COREX algorithm. The different distribution and ranges of local stabilities of the *Anabaena* and *H. pylori* apoflavodoxins explain the essential experimental differences observed: much lower T_{m1}, greater resistance to global unfolding and more pronounced cold denaturation in *H. pylori*. Finally, a new strategy is proposed to identify using COREX structural characteristics of equilibrium intermediate states populated during protein unfolding.

Keywords

flavodoxin; *Helicobacter pylori*; protein stability; equilibrium phase diagram; partially unfolded intermediate; ligand binding

Flavodoxins are α/β. proteins involved in a variety of redox reactions (1). They are composed of a 5-stranded, parallel β-sheet surrounded by α-helices, and they bear a non-covalently bound cofactor, flavin mononucleotide (FMN), where the redox properties reside. Flavodoxins can be classified in two classes: short-chain and long-chain ones, the latter containing a 20-residue loop, of a still unclear function, inserted in the fifth β-strand (2,3). One interesting characteristic of flavodoxins is that, upon removal of the flavin cofactor, the apoprotein remains folded (4,

Corresponding author: jsancho@unizar.es, Phone: 34 976761286, Fax: 34 976762123.

5). The flavodoxins from several non-pathogenic bacteria have been used to investigate protein stability in connection with ligand binding (*Anabaena PCC7119* (6-9); *Azotobacter vinelandii* (10,11); *Desulfovibrio desulfuricans* (12); *Desulfovibrio vulgaris* (13)). Work in our laboratory on *Anabaena* flavodoxin has shown that the cofactor increases the cooperativity of the thermal unfolding (which is three-state for the apoprotein and two-state for the holoprotein) because it binds at the weak region of the apoprotein that becomes unstructured at a temperature lower than that of the global unfolding (9). In other flavodoxins, however, the cofactor does not seem to modify the number of macroscopic states that can be observed at equilibrium. This different influence of cofactor binding in equilibrium unfolding cooperativity, which may be related to differences in the strength of the complexes involved or to structural differences in the apoproteins, deserves further investigation.

Flavodoxins are also found in pathogenic bacteria (1), i.e. *Helicobacter pylori*, a Gram-negative bacterium related with several digestive diseases, such as type B gastritis, stomach and duodenal ulcers (14), adenocarcinomas (15) and stomach lymphomas (16). *H. pylori* is found colonizing the stomach of 50% of the human population (17), although only around 20% of the infected individuals develop pathologies. Recently, flavodoxin has been shown to be essential for the survival of *H. pylori* because it participates as the electron acceptor of the pyruvate:flavodoxin oxidoreductase complex (PFOR) in an essential pathway that catalyzes pyruvate oxidative decarboxilation (18,19). This has open the possibility to use the protein as a target for developing new inhibitory drugs against the bacterium (20). *H. pylori* flavodoxin, is a long-chain flavodoxin. It contains 164 residues and shares 44% sequence identity with *Anabaena PCC7119*, 39% with *Azotobacter vinelandii* and 29% with *Desulfovibrio desulfuricans* and *Desulfovibrio vulgaris* flavodoxins. The x-ray structure of the *H. pylori* protein reveals (18) that a tryptophan residue typically involved in cofactor binding in many flavodoxins appears replaced by an alanine, which creates a distinct pocket near the *si*-face of the redox cofactor (20). The structure of the apo form (PDB code: 2bmv) has also been recently determined (21) and it is similar to that of the holoprotein, except at the FMN binding site.

We report here a structure-stability study of *H. pylori* flavodoxin as a step towards using the holoprotein as a drug target in high throughput thermal up-shift screening assays (20,22) and as a contribution to understanding the interplay between intrinsic and cofactor-driven stability in the flavodoxin family. The apoprotein from *H. pylori* displays a higher thermostability towards full unfolding than other known apoflavodoxins but, surprisingly, a lower cooperativity, which allows to observe the accumulation of two partially-unfolded equilibrium intermediates, the first one similar to the thermal intermediates described for other flavodoxins (1,10,23), and the second one much closer to the unfolded state. The structural reason of this different distribution of partly unfolded conformations near the native basin (24), compared with other flavodoxins so far studied, is here investigated using the COREX algorithm (25-27) and it appears to originate from *H. pylori* flavodoxin combining a more stable core with a wider range of local stabilities. The structural-energetic analysis performed helps to explain why *H. pylori* flavodoxin begins its complex thermal unfolding at lower temperatures, appears to present a more pronounced cold denaturation, and does not exhibit the cooperative two-state behavior observed in *Anabaena* flavodoxin when the FMN cofactor is bound. In addition we propose a new method using the COREX algorithm that seems to identify the week regions that become unfolded in the major thermal intermediate that is found in all long-chain flavodoxins so far analyzed.

Materials and Methods

Protein purification, determination of extinction coefficients and spectroscopic characterization

Recombinant *H. pylori* flavodoxin was purified as described (20) and a mixture of holo and apo forms was obtained. Apo and holoflavodoxin dissolved in 50 mM Tris-HCl, pH 8.0 were separated in a MonoQ10 column (*FPLC, Amersham*), equilibrated in the same buffer, using a linear 0 to 1 M NaCl gradient. Apoflavodoxin can also be obtained by removing the flavin mononucleotide group from the holoprotein by treatment with trichloroacetic acid (28). The molar extinction coefficient of *H. pylori* apoflavodoxin, at 278 nm in 50 mM MOPS, pH 7, was determined to be 15 960 $M^{-1}.cm^{-1}$ from its amino acid composition and its absorbance in that buffer and in 6 M guanidine hydrochloride (29). For holoflavodoxin, a molar extinction coefficient at 452 nm of 10 650 $M^{-1}.cm^{-1}$ in 50 mM Tris-HCl pH 8 was used (20). Far-UV and near-UV circular dichroism (CD) spectra were acquired at pH 7.0 and 9.0, in both native (25 ± 0.1 °C) and denaturing conditions (90 ± 0.1 °C), using a *Jasco 710* spectropolarimeter. For near-UV CD, a 1-cm path length cuvette was used with 20-40 μM protein solutions and 50 mM buffers. For far-UV CD, the path length was 0.1 cm, protein concentration was 20 μM, and MOPS pH 7.0 or EPPS pH 9.0 buffers (containing in addition either 20 or 45 mM NaCl, respectively) were used at a 5 mM concentration.

Thermal unfolding followed spectroscopically

Thermal denaturation was followed by fluorescence and circular dichroism in several spectral regions. Fluorescence emission spectra (from 300 to 400 nm, with excitation at 280 nm) were acquired and the average energy of emission (30,31) used to follow the unfolding: The unfolding by circular dichroism was followed at single wavelengths in the far-UV (222 nm), near-UV (291 nm) and visible (373 nm) regions. Apoflavodoxin concentration was 2-20 μM for fluorescence measurements, 20 μM for far-UV and 20-40 μM for near-UV CD in two conditions: 50 mM MOPS, pH 7.0 and 50 mM EPPS, pH 9.0. Holoflavodoxin concentration was 20 μM in all cases.

Individual thermal unfolding curves of apoflavodoxin were fitted to a three-state equation as described (23)assuming that the spectroscopic signals of the folded, intermediate and unfolded states vary linearly with temperature. However, the slopes of the signal of the intermediate are fixed to zero because, since it never accumulates to 100 % over a significant temperature range, they cannot be determined accurately and allowing their fitting would increase parameter dependency of other fitting parameters. Since the individual spectroscopic curves do not superimpose one on another, they were globally fitted to a four-state equation:

$$S=\frac{S_N+m_N T+S_{I1}e^{-\Delta G_1/RT}+S_{I2}e^{-(\Delta G_1+\Delta G_2)/RT}+(S_U+m_U T)e^{-(\Delta G_1+\Delta G_2+\Delta G_3)/RT}}{1+e^{-\Delta G_1/RT}+e^{-(\Delta G_1+\Delta G_2)/RT}+e^{-(\Delta G_1+\Delta G_2+\Delta G_3)/RT}} \quad (1)$$

where S_N, S_{I1}, S_{I2}, and S_U are the spectroscopic signals of the native state, first and second intermediate states, and denatured states. ΔG_i are calculated as described in (23).

For holoflavodoxin, some individual thermal unfolding curves could be fitted to a two-state model (near-UV and visible CD) and some others had to be fitted to a three-state model (UV fluorescence and far-UV CD). In addition, all the curves were globally fitted to a four-state equation (equation 1).

Differential scanning calorimetry

The heat capacity of flavodoxin was measured as a function of temperature with a differential scanning VP-DSC microcalorimeter (*Microcal* LLC., Northampton, MA). Protein samples and

reference solutions were degassed and carefully loaded into the cells to avoid bubble formation. The baseline of the instrument was routinely recorded before the experiments with both cells filled with buffer. Thermal denaturation scans of apoflavodoxin were performed with 50 μM protein solutions in 50 mM MOPS pH 7.0, 50 mM Hepes pH 8.0 50 mM Hepes pH 8.5, and 50 mM EPPS, pH 9.0, at a scanning rate of 1°C/min from 10 to 100 °C. The ionic strength of all samples was between 40-45 mM, except for the pH 7.0 experiments, where it was 20 mM to allow a more direct comparison with data available for flavodoxins from other species. DSC profiles at different protein concentrations and scanning rates were recorded to ensure that no kinetic effects or oligomerization processes were present. Reversibility of the unfolding was checked by sample reheating after cooling inside the calorimetric cell and, in all cases, was higher than 80%. For holoflavodoxin DSC experiments, a 40 μM protein solution in EPPS 50 mM pH 9.0 was used.

DSC data was fitted to three-state and four-state equations (32), where the excess heat capacity change was analyzed considering a sequential unfolding model (32). The partition function in such model is given by:

$$Q=1+e^{-\Delta G_1/\mathrm{RT}}+e^{-(\Delta G_1+\Delta G_2)/\mathrm{RT}}+e^{-(\Delta G_1+\Delta G_3+\Delta G_3)/\mathrm{RT}} \tag{2}$$

from which, using the Gibbs-Helmholtz relationship, the average excess enthalpy and heat capacity are calculated:

$$\begin{aligned}\langle\Delta H\rangle&=\frac{\sum_{i=1}^{3}\left(e^{-\left(\sum_{j=1}^{i}\Delta G_j\right)/\mathrm{RT}}\left(\sum_{j=1}^{i}\Delta H_j\right)\right)}{Q}\\ \langle\Delta C_P\rangle&=\frac{\partial\langle\Delta H\rangle}{\partial T}\end{aligned} \tag{3}$$

Statistical mechanical deconvolution (see below) was used to analyze the excess unfolding enthalpy, while the van't Hoff enthalpy, ΔH_{vH}, was calculated as described (33). The analysis of the unfolding transitions in the presence of cofactor is a generalization of the procedure for the apo-protein. If the cofactor only binds to the native state, the partition function is:

$$Q=1+\frac{e^{-\Delta G_1/\mathrm{RT}}}{1+K_B[L]}+\frac{e^{-(\Delta G_1+\Delta G_2)/\mathrm{RT}}}{1+K_B[L]}+\frac{e^{-(\Delta G_1+\Delta G_2+\Delta G_3)/\mathrm{RT}}}{1+K_B[L]} \tag{4}$$

where K_B and [L] are the ligand binding affinity and free concentration, respectively. The denominator in the last three terms is the ligand binding polynomial. Then, applying again the Gibbs-Helmholtz relationship, the excess average enthalpy and heat capacity are calculated:

$$\begin{aligned}\langle\Delta H\rangle&=\frac{\sum_{i=1}^{3}\left(\frac{e^{-\left(\sum_{j=1}^{i}\Delta G_j\right)/\mathrm{RT}}}{1+K_B[L]}\left(\sum_{j=1}^{i}\Delta H_j-\langle\Delta H_B\rangle\right)\right)}{Q}\\ \langle\Delta C_P\rangle&=\frac{\partial\langle\Delta H\rangle}{\partial T}\end{aligned} \tag{5}$$

where $\langle\Delta H_B\rangle$ is the average binding enthalpy for the native state (34).

Including explicitly the temperature dependence of the binding constant and the binding enthalpy, assuming a constant heat capacity change upon binding, it is possible to estimate the thermodynamic parameters for cofactor binding from temperature denaturation experiments performed at different cofactor concentrations (34).

Statistical Mechanical Deconvolution

This method (32,35) allows to obtain the thermodynamic parameters for the thermal unfolding transitions of a protein from the average excess enthalpy function of the system, $<\Delta H>$, without any *a priori* assumption of a particular unfolding model. The average excess enthalpy $<\Delta H>$ as a function of temperature is obtained from DSC data by direct integration of the excess heat capacity function, which is the direct observable, and the partition function of the system can be calculated as:

$$Q(T)=\exp\int_{T_0}^{T}\left(<\Delta H>/RT^2\right)\mathrm{dT} \tag{6}$$

From the partition function, the number of discrete macroscopic energy states together with their thermodynamic parameters can be estimated in a recursive procedure (35).

Spectra deconvolution

The spectroscopic properties of the macroscopic states of *H. pylori* apoflavodoxin that become significantly populated during the thermal unfolding have been determined by deconvolution of spectra recorded at different temperatures, using the following equation:

$$Y(\lambda,T)=Y_N(\lambda,T)X_N(T)+Y_{I_1}(\lambda,T)X_{I_1}(T)+Y_{I_2}(\lambda,T)X_{I_2}(T)+Y_U(\lambda,T)X_U(T) \tag{7}$$

where the observed value of a given spectroscopic measurement at a certain wavelength and temperature, $Y(\lambda,T)$, is a linear combination of the values of the different states, $Y_i(\lambda,T)$, and their populations, $X_i(T)$, that are calculated at each temperature from the free energy values ΔG_1, ΔG_2 and ΔG_3 obtained by global fitting of the unfolding curves to the sequential four-state model.

FMN binding to apoflavodoxin

The interaction between apoflavodoxin and its FMN cofactor has been studied in 50 mM MOPS pH 7 and in 50 mM EPPS, pH 9 by fluorescence spectroscopy (monitoring intrinsic FMN fluorescence as described (7)) and isothermal titration calorimetry (ITC). Isothermal titration calorimetry was performed using a VP-ITC calorimeter (Microcal LLC, Northampton, MA.). A 10 μM flavodoxin solution present in the calorimetric cell was titrated with FMN dissolved in the same buffer (90 μM in the injection syringe). Both solutions were previously degassed. A time between injections of 700 seconds was required to recover the baseline, specially at the end of the titration experiment. Data analysis was performed with software developed in our laboratory. On the other hand, the quenching of flavin fluorescence at 525 nm upon adding small aliquots of apoflavodoxin was recorded at 11, 15, 20 and 25 °C in order to calculate the van't Hoff binding enthalpy, ΔH_B (7), which has been compared with that obtained by ITC.

Structure-based thermodynamic calculations

Structure-based calculations were performed using a previously published empirical parameterization of the unfolding energetics, based on changes in polar and apolar surface area (ΔASA_{pol} and ΔASA_{ap}) (36,37) upon unfolding. The heat capacity change is parameterized as (38,39).

$$\Delta C_P=\Delta C_{P,ap}+\Delta C_{P,pol}=a(T)\cdot\Delta ASA_{ap}+b(T)\cdot\Delta ASA_{pol} \tag{8}$$

The COREX algorithm

The COREX algorithm provides a way of generating an ensemble of partially folded states of a protein, using the high resolution native structure as template (25-27). The entire protein is

considered as composed of different folding units, and partially folded states are generated by unfolding these units in all possible combinations (also called partitions). The COREX algorithm, thus, produces a list of possible conformations and their respective probabilities. The stability of each residue is then defined as the ratio between the number of conformations in which it is in the native state and the number of conformations in which it is unfolded, where each conformation is weighted by its energy.

Results

Spectroscopic characterization of *H. pylori* apo and holoflavodoxin at pH 7.0 and 9.0

At both pHs, the apo and holo forms of the protein show very similar far-UV CD spectra (Figure 1a), suggesting that all the secondary structure elements are retained in the apoprotein. The near-UV CD spectra of the holo and apo forms are, in contrast, quite different (Figure 1b). The apo form displays two small peaks of much lower intensity than that of the peaks in the spectrum of *Anabaena* apoflavodoxin (6). This is not surprising because the *H. pylori* protein lacks the W120/W159 pair, which is the main contributor to the *Anabaena* near-UV CD spectrum (40). When FMN is bound to the protein, the near-UV CD spectrum is more intense, very likely reflecting direct contributions from the cofactor. The CD data together suggests that the apoprotein is well-folded, as indicated by its x-ray structure (21).

Thermal unfolding of *H. pylori* apoflavodoxin

The thermal unfolding has been followed at both pH 9.0 and 7.0 (Figures 2a and 2b, respectively) using far-UV CD, near-UV CD and tryptophan fluorescence emission. On the other hand, DSC thermograms of apoflavodoxin have been recorded at pH 7.0, 8.0, 8.5 and 9.0 (Figures 2c and 2d). Spectroscopic and DSC reversibility experiments were performed, that allowed to recover the original curve shapes with around 80% of the initial signal, which means that the thermal unfolding is at least 80% reversible. Besides, protein association was ruled out because the same DSC or spectroscopic thermal unfolding curves were obtained using 2, 20 and 40 μM protein concentrations at all pH values investigated (data not shown). Then, the native state is monomeric.

At pH 9.0, the spectroscopic unfolding curves show two well defined transitions (Figure 2a), which is indicative of, at least, a three-state behavior. Indeed, all spectroscopic unfolding curves can be individually fitted to a three-state model (Table 1). However, the curves obtained at pH 7.0 show somewhat less cooperative transitions (Figure 2b) and, when they are individually fitted to three-state equations, the higher temperature transitions do not coincide. Accordingly, the spectroscopic data at pH 7 have been directly fitted to a four-state model (Table 1).

The thermal unfolding equilibrium has been further investigated by DSC at pH 7.0, 8.0, 8.5 and 9.0 (Figure 2c). The profiles at pH 8.0, 8.5 and 9.0 are very similar, with two prominent peaks: the high temperature one shifting to lower temperatures as the pH increases, and the other peak remaining almost unchanged. At pH 7.0, however, the curve displays a different behavior with a very low enthalpy change and a lower resolution of the two peaks (the second peak is wider at pH 7.0 than at higher pHs), likely indicating the presence of an additional transition. Since theses differences at pH 7.0 could be due to the slightly lower ionic strength present in the pH 7.0 solution (see methods), the thermogram was also recorded at 50 mM ionic strength and the same behavior was evident (data not shown). Based in the above observations we have selected pH 9.0 for further analysis and comparison with the spectroscopic data because the errors associated to the fitted parameters are much lower than those obtained at pH 7.0. From the raw DSC data at pH 9.0, the experimental baseline and the heat capacity of the native state (first or second order polynomial in temperature) were subtracted to obtain the excess heat capacity change. A heat capacity change for the unfolding process has to be

assumed. Usually, several DSC experiments at different but close pH values are performed from where the slope of a ΔH_m vs T_m plot, ΔC_P, is determined. However, in a protein exhibiting several unfolding transitions, such approximation is hard, if not impossible. Instead, we have calculated, from a structure-based parameterization (36-38) (equation 8), a theoretical heat capacity change of 2.7 kcal.mol^{-1}.K^{-1} for the global unfolding process of *H. pylori* apoflavodoxin. This value is close to the one calculated for *Anabaena* apoflavodoxin (2.8 kcal.mol^{-1}.K^{-1}) and similar to the two experimental reported values for this protein, 2.5 ± 0.3 kcal.mol^{-1}.K^{-1} and 3.1 ± 0.8 kcal.mol^{-1}.K^{-1} (41). Once the excess heat capacity curve was obtained (Figure 2d, open circles), it was first analyzed using a three-state model (gray line), but the fit was poor. A four-state model greatly improved the fit (black line).

To further test the appropriateness of the four-state model, a statistical mechanical deconvolution (35) of the DSC data was performed in order to calculate, from the average excess enthalpy function of the system, $<\Delta H>$, as a function of temperature, the minimum number of discrete macroscopic energy states. The excess heat capacity data, was, thus, converted into $<\Delta H>$ data by direct temperature integration and the result is shown as thick gray line in Figure 3. The additional lines in the figure represent the excess enthalpy change after the contribution of each unfolding transition is eliminated using a recursive method (see Materials and Methods). The analysis shows that three transitions need to be considered before a linear temperature dependency of the enthalpy is obtained (thin black line in Figure 3 at high temperature) as characteristic of the enthalpy function of a unique state (the denatured state). Statistical mechanical deconvolution, thus, confirms the presence of four different states in the thermal unfolding equilibrium of *H. pylori* apoflavodoxin at pH 9.0. The same result was obtained for pH 7.0 (not shown).

In principle, a four-state unfolding equilibrium could give rise to three peaks in a DSC curve. The reason why only two peaks are evident in the thermogram was investigated as follows. The lower temperature distinct peak was fitted to a two-state model and the fitted curve was subtracted from the original one, leading to a curve that contains only the contributions from the second distinct peak observed at high temperature. Once the contributions of the peaks were separated, the ratio between van't Hoff and calorimetric enthalpies of each peak was determined. While the first peak yielded a $\Delta H_{vH}/\Delta H_{cal}$ ratio of 1.05, indicating that it corresponds to just one thermal unfolding transition, the second peak showed a ratio of 0.58, suggesting that it corresponds to, at least, two close unfolding transitions.

The thermodynamic parameters obtained from both calorimetric and spectroscopic analysis are compared in Table 1. The thermodynamic parameters obtained from either the far-UV CD or the fluorescence curves agree with those obtained from a van't Hoff analysis of the DSC data, which indicates that those techniques are unable to resolve the last two close thermal transitions. In contrast, the high temperature transition observed in the near-UV CD curve corresponds to the second transition of the DSC curve rather than to an average of the second and third transitions.

FMN binding

The stabilizing effect associated to FMN binding has been studied for several flavodoxins with conflicting results, as recently summarized (1,9). For a complete characterization of the binding of FMN to *H. pylori* apoflavodoxin, both ITC and spectroscopic techniques have been used. While ITC is the technique of choice to obtain the affinity in the 10^2 to 10^7 M^{-1} range of dissociation constants, spectroscopic techniques are preferred, if available, for stronger complexes (7). Still, ITC provides for the latter ones more precise values of enthalpy and heat capacity changes of binding. Figure 4 shows a titration of FMN fluorescence with apoflavodoxin at 25 °C (Figure 4a) and the heat liberated by FMN injections to an apoflavodoxin solution at the same temperature (Figure 4b). The K_d obtained from the

spectroscopic titration, which for this complex is more accurate, is at least one order of magnitude higher than that determined for the *Anabaena* protein (7), as can be expected from the larger solvent exposure of the FMN molecule in the *H. pylori* complex. The K_d value obtained by ITC is slightly higher than the spectroscopic one (6.8 nM by spectroscopy, 27 nM by ITC and 10 nM by DSC), which is likely due to the fact that the K_d is in the limit for ITC determination. Besides, in the last injections of the ITC experiment, some extra time is needed to recover the baseline and not all the thermal effect upon binding might be recorded in those injections, suggesting that kinetic effects could be distorting the ITC titration.

The enthalpy of binding, as determined by ITC, is of - 21 kcal/mol at pH 7.0 and very similar at pH 9.0 (Table 2). To estimate spectroscopically the binding enthalpy, the fluorescence quenching of FMN by the apoprotein was measured at 11, 15 and 20 °C. The corresponding binding constants were determined and the enthalpy of binding was calculated from the van't Hoff relationship. The estimated enthalpy is lower than the one obtained by calorimetric titration, although the discrepancy is not large. It should be bore in mind that the spectroscopically determined binding enthalpy is less reliable and more affected by errors. In order to find out if protonation effects are affecting the enthalpy obtained by calorimetry, ITC experiments were performed at the same pH and temperature using buffers with different ionization enthalpies, ΔH_{ion} (data not shown). The linear regression of the data ΔH_{app} vs ΔH_{ion} provides information about proton exchange between complex and solvent upon ligand binding, that is, the number of protons bound or released upon ligand binding, n_H, and the buffer-independent binding enthalpy, ΔH_B, according to:

$$\Delta H_{app} = \Delta H_B + n_H \Delta H_{ion} \quad (9)$$

At pH 7.0 and pH 9.0, the n_H parameter obtained after fitting the data to equation 9 was 0.1 and -0.2 (± 0.2), respectively. Therefore, the net proton exchange coupled to ligand binding is small and the measured binding enthalpy by ITC does not include a significant contribution from buffer ionization or any ionizable group in the protein.

The favorable binding enthalpy overcomes the unfavorable entropy change that takes place upon cofactor binding. The negative value of the binding entropy in *H. pylori* flavodoxin means that the freezing of the FMN molecule and of the interacting protein residues in the complex is not compensated by the expected concomitant release of water molecules that must take place during cofactor binding. As it will be discussed below, the binding site of *H. pylori* apoflavodoxin presents a lower local stability than that of *Anabaena* for which the overall entropic contribution to binding is favorable. That lower local stability may introduce a greater conformational entropy cost in the *H. pylori* complex, which adds to an expected smaller contribution of the hydrophobic effect. In *Anabaena* flavodoxin, however, both enthalpic and entropic contributions are favorable (Table 2), which gives rise to a higher affinity in spite of a less favorable enthalpy. It is interesting to compare the *H. pylori* FMN binding energetics with those of the *Anabaena* flavodoxin W57A mutant (Table 2), which exhibits a cofactor solvent-accesibility similar to that in the *H. pylori* complex (7,21). The affinity for FMN of the two apoproteins is similar, as it is similar the heat capacity change, related to the surface area buried upon binding. Nevertheless, the thermodynamic contributions are differently compensated. In the *Anabaena* mutant, the binding enthalpy is much less favorable than in *H. pylori* and the entropy value is positive and even more favorable than in the wild-type *Anabaena* protein.

Thermal unfolding of flavodoxin

The effect of FMN binding in protein stability was directly evaluated by recording the thermally-induced unfolding of the holoprotein (at equimolecular concentration of FMN and protein) at pH 7.0 and, in more detail, at pH 9.0. Spectroscopically, the average energy of the

fluorescence spectra, far-UV CD, near-UV CD and visible CD signals were used to follow the thermal denaturation (Figure 5a and 5b). While the near-UV and visible CD curves, reflecting contributions from the FMN cofactor, are superimposable and can be fitted to a simple two-state model, the two other spectroscopic curves need to be fitted to a three-state model and, in addition, they cannot be superimposed with each other. The minimal model is, thus, four-state. As observed in apoflavodoxin, the holoprotein displays poorly defined unfolding transitions when is monitored by fluorescence and far-UV CD, specially at pH 7.0, due to the low enthalpy value associated to the last two transitions (Table 3). DSC experiments of holoflavodoxin were also performed at pH 9.0 (Figure 5c). The calorimetric curve shows a single broad peak, indicating that the three transitions are closer than in apoflavodoxin. The ratio between van't Hoff and calorimetric enthalpies is of 0.38, meaning that at least two transitions are masked in the peak. However, the thermogram cannot be fitted to a three-state sequential unfolding model and a four-state one is required. Thus, in contrast with what was observed for *Anabaena* flavodoxin (9), in *H. pylori* flavodoxin the stabilization induced by FMN binding does not decrease the number of macroscopic states that become significantly populated during thermal unfolding. If FMN concentration is increased with respect to the protein, the protein is further stabilized and the cooperativity (measured as the van't Hoff/calorimetric enthalpies ratio) increases (see Discussion). As seen for apoflavodoxin (Table 1), there is a good correlation between the thermodynamic parameters obtained spectroscopically and calorimetrically. In fact, the small differences in T_{m1} are very likely due to the higher concentration of holoprotein in the DSC experiments (see Materials and Methods).

Discussion

Thermodynamic and spectroscopic characterization of the four states of *H. pylori* flavodoxin that populate along the thermal unfolding equilibrium

Both calorimetry and a variety of spectroscopic techniques used to investigate the thermal unfolding equilibrium of apoflavodoxin reveal it is a complex process with three distinct transitions, yielding to the appearance of four different states, in contrast to other known flavodoxins. The agreement between the spectroscopic global fit and the calorimetric analysis is excellent both in T_ms and enthalpy changes, although the spectroscopic fit gives rise to large errors for the second transition. The native state of apoflavodoxin never populates to 100% (its maximal accumulation is of around 85 % at 280 K; Figure 6a) as a consequence of a pronounced cold-denaturation caused by the first unfolding transition displaying a low enthalpy change (about 25% of the N-to-U enthalpy change) combined with a fairly high heat capacity change (around 1.2-1.3 $kcal.mol^{-1}.K^{-1}$). Cold denaturation has also been observed, although less pronounced, in *Anabaena* apoflavodoxin (41), whose thermal unfolding follows a three-state model where the first transition displays enthalpy and heat capacity changes (41) very close to those determined for the first transition in the *H. pylori* protein. It is thus tempting to identify the first thermal intermediate of *H. pylori* apoflavodoxin (I_1) with the single unfolding intermediate observed in *Anabaena*, the structure of which has been characterized by equilibrium Φ-analysis and NMR (23). This intermediate essentially adopts a native conformation where the long-loop characteristic of long-chain flavodoxins, together with, at least, two of the three-FMN binding loops (those involved in the binding of the isoalloxacine moiety) are unfolded. The intermediate, thus, retains most of the secondary structure. To test whether the first intermediate of *H. pylori* apoflavodoxin thermal unfolding corresponds with the well characterized single thermal intermediate in *Anabaena* (23), we have determined the individual fluorescence, far and near-UV circular dichroism spectra of the four macroscopic states that populate along the thermal unfolding by deconvolution of the apoflavodoxin spectra recorded at different temperatures (Figure 7). The fluorescence spectrum of I_1 is close in intensity to the native spectrum, although the maximal intensity appears at 328 nm, rather than at 320 nm as in the native state. Therefore, there is a slight increase in solvent-exposure of

some of the tryptophan residues in this intermediate. This different local environment of the tryptophans is also evidenced in a distorted near-UV CD spectrum, as compared with the native one. Nevertheless, there is still some near-UV CD signal, which means that at least one of the two tryptophans in the protein remains in an asymmetric environment in I_1. In fact, the two tryptophan residues are located in regions that are expected to be folded if I_1 is structurally similar to the *Anabaena* intermediate (23). Finally, the far-UV CD spectra indicate that I_1 preserves most of its native secondary structure (around 80% of the native helix content). All the spectroscopic information is thus consistent with I_1 being similar to the single thermal intermediate observed in the *Anabaena* apoflavodoxin. In contrast, the spectra of I_2 indicate that the tertiary contacts have been lost together with a large amount of the secondary structure (significantly α-helix), and there is a considerable increase in solvent-exposure of the tryptophan residues, with the maximum of fluorescence intensity at 339 nm. In fact, the unfolding of I_1 to yield I_2 involves a significant change in heat capacity. However, the blue-shifted fluorescence spectrum (339 nm) relative to the 349 nm in the denatured state indicates that at least one of the two tryptophan residues is still partially buried. In addition, the far-UV CD spectra suggests that around 25 % of native-helix content and 50 % of native-β-sheet content is retained in I_2. Although the heat capacity of I_2 is not far from that of the unfolded state, its high enthalpy of unfolding suggests that it may still contain a partially folded region. One possibility is that this intermediate is organized around a region of the protein with a particularly high local stability. This additional intermediate has not been observed in other flavodoxins. Finally, the third transition, exhibiting a smaller change in heat capacity but a substantial enthalpy change, represents the unfolding of I_2 to the unfolding state. This latter state shows some signal around 222 nm (compared to the spectra of the chemical-unfolded state, not shown), which seems to indicate that the thermally unfolded state may still retain some residual helical structure. It is possible that such residual structure could be related to the high local stability of the third α-helix, as calculated by the COREX algorithm (not shown) and described for *A. vinelandii* apoflavodoxin in hydrogen exchange experiments (42).

As it has been described for *Anabaena* apoflavodoxin (6), *H. pylori* apoflavodoxin presents, at acidic pH, a molten globule conformation (work in progress). However, neither of the two thermal intermediates described in this work display molten globule spectroscopic characteristics, since the first one preserves some tertiary contacts and the second one displays a marked debilitation of the secondary structure.

Preferential stabilization of the apoflavodoxin native state by FMN binding

The affinity of the complex between FMN and apoflavodoxin from *H. pylori* is high (-10-11 kcal/mol), but lower than in the two other long-chain flavodoxins studied (9,11). Compared to the *Anabaena* complex, the lower affinity of the *H. pylori* one is due to a more favorable enthalpy of binding which is offset by an unfavorable entropy change. The entropy loss in the *H. pylori* complex is not surprising. On the one hand, an alanine residue replaces the highly conserved tryptophan residue present in most flavodoxins, which makes the FMN molecule much more accessible to solvent (156.3 $Å^2$ in *H. pylori* versus 107.4 $Å^2$ in *Anabaena*) (43). Since in both complexes the vast majority of this exposed area (more than 90 %) corresponds to apolar groups of the FMN molecule, the contribution of the hydrophobic effect to the stability of the *H. pylori* complex is lower than that in the *Anabaena* one. On the other hand, the greater exposure of the FMN binding pocket in the *H. pylori* apoprotein might, in principle, allow a larger rotational entropy of neighboring residues in the absence of the cofactor, which would be lost in the complex. This is consistent with the low T_m displayed by the first thermal transition in *H. pylori* apoflavodoxin that leads to I_1. Since it appears that this intermediate is structurally equivalent to the one previously analyzed in *Anabaena* (23), it should present a disordered binding site. It seems therefore that the binding site in *H. pylori* apoflavodoxin may

display a lower local stability (also predicted by COREX analysis; see below), which is consistent with a greater flexibility and higher entropy penalty for complex formation.

H. pylori flavodoxin lacks some of the residues that establish important interactions in the *Anabaena* complex; significantly, one of the aromatic residues involved in aromatic stacking with FMN (Trp57 in *Anabaena*) and one threonine residue (Thr15 in *Anabaena*) hydrogen bonded to the phosphate moiety of the cofactor. In *Anabaena*, mutating these residues (W57A or T15V; see Table 2) destabilizes the complex by around 2 kcal/mol (7). Besides, the W57A replacement moves the binding enthalpy from −12 to −7 kcal/mol. It is thus remarkable that the enthalpy of binding of the *H. pylori* complex is much more favorable than that of the *Anabaena* one. This could be also connected with the greater flexibility at the binding site. Concomitant with a lost of entropy, cofactor binding would strengthen internal protein interactions leading to a marked, though not full, entropy/enthalpy compensation. Thus, the observed binding enthalpy would correspond to the intrinsic binding enthalpy at an ordered binding site plus the refolding enthalpy of the disordered binding site.

Native state-specific stabilization by ligand binding can lead to a sharp increase in unfolding cooperativity, as it has been observed for *Anabaena* flavodoxin (9) where the three-state behavior of the apoprotein changes to two-state in the presence of equimolecular amounts of FMN. Clearly, the stabilizing influence of the cofactor in the three unfolding transitions observed in *H. pylori* is very different, as can be seen by comparing the corresponding T_m values of apo and holoflavodoxin (Tables 1 and 3). In fact, the last two transitions take place at very similar temperatures, which strongly suggests that the cofactor dissociates in the first transition, the T_m of which is greatly increased upon FMN binding. There are, nevertheless, slight variations in T_{m2} and stronger ones in ΔH_2.

To test the consistency of our proposal that the cofactor is released in the first unfolding transition, we have recorded thermograms (Figure 8) of the holoprotein in the presence of excess FMN (2, 3, 10 and 20-fold molar excess of FMN). These, together with the thermogram corresponding to the apoprotein under identical solution conditions, have been globally fitted to a sequential unfolding model where the cofactor is released in the first unfolding transition, that is, the cofactor only binds to the native state. The thermodynamic parameters corresponding to cofactor binding can be obtained from the global analysis. The ligand binding heat capacity was fixed to a reasonable estimate of −0.3 kcal/K·mol; otherwise high parameter correlation in the fitting process would arise. The actual ligand binding heat capacity value cannot be determined reliably from these experiments and does not affect significantly the results. The estimated values at 25°C for the binding affinity and the binding enthalpy of the native state, $1.0 \cdot 10^8$ M^{-1} and −14 kcal/mol, respectively, are in good agreement with the values determined independently by isothermal titration calorimetry under similar experimental conditions ($K_B = 6.4 \cdot 10^7$ M^{-1} and ΔH_B = -23.1 kcal/mol), considering the extrapolation errors.

The population of accessible states along the thermal unfolding in the apo and holo forms (Figure 6a and 6b, respectively) shows that FMN binding increases the population of the native state and widens its stability window. In fact, the native state is by large the most stabilized state upon FMN binding, which increases the energy gap with the first intermediate without hardly modifying the two subsequent transitions. The fact that FMN binding increases the relevant stability of the protein ($N \leftrightarrow I_1$ equilibrium) (44), while leaving the residual stability of the partly unfolded conformations ($I_1 \leftrightarrow I_2 \leftrightarrow D$) unchanged is consistent with I_1 displaying a structure similar to that characterized for the single thermal intermediate that appears in the thermal unfolding of the apoflavodoxin from *Anabaena* (23). That in *H. pylori* flavodoxin the binding of the cofactor does not lead to a highly cooperative two-state unfolding is simply due to the lower relevant stability and the higher residual one of the *H. pylori* apoprotein, compared to the *Anabaena* one, together with the lower affinity of FMN binding.

A temperature-ligand concentration phase diagram for *H. pylori* flavodoxin thermal unfolding

The coupling of the conformational and binding equilibria in the flavodoxin-FMN system is naturally illustrated in the temperature-ligand concentration phase diagram in Figure 9. The solid lines are constructed, using the thermodynamic parameters determined for unfolding and FMN binding at pH 9.0 (Table 1 and 2), as the geometric sites of the points at which a given species populates 50% of the total protein concentration (45). The lines thus engulf regions where a given species is dominant. The intercepts with the upper x-axis correspond to the Tm's of the different individual unfolding transitions of flavodoxin in the absence of FMN, whereas the intercept with the left y-axis indicates the logarithm of the (apparent) FMN binding affinity at the lower temperature in the diagram. The NL line represents the temperature dependency of the logarithm of the dissociation constant. The traces starting from the Tm's and following the NL line represent the ligand concentration dependence of the Tm's. The two lines between N and NL do not coincide because a significant percentage of non-native and non-liganded protein is present even at low temperature. The two dotted straight lines predict the arising of the different conformations observed in typical temperature denaturation experiments performed in the absence (top line) and the presence (bottom line) of FMN such as those giving rise to the population diagrams in Figure 6. The diagram indicates that at physiological FMN concentrations, the two intermediates will populate in thermal unfolding, and that full unfolding cooperativity, such as that observed in *Anabaena* flavodoxin (9), where only the liganded and the unfolded protein coexists, can only be achieved at FMN concentrations above 1 M. As the FMN concentration increases, the first intermediate I_1 will be less populated during a temperature denaturation, indicating a more cooperative unfolding where the relevant stability ($N \leftrightarrow I_1$) is increased, as mentioned before.

Why *H. pylori* thermal unfolding is less cooperative? A COREX analysis

The thermal unfolding of two long-chain apoflavodoxins (from *Anabaena* (9,41) and from *Azotobacter vinelandii* (10)) and one short-chain one (from *Desulfovibrio desulfuricans* (12)) have been described. The three proteins display a three-state thermal unfolding equilibrium, for which they exhibit similar thermodynamic parameters. Surprisingly *H. pylori* apoflavodoxin, with an average 37% sequence identity and 52 % similarity with the three other proteins, follows a four-state model with an additional intermediate. To identify the structural features that give rise to the observed reduced cooperativity towards thermal unfolding, a structure-stability comparison of the *H. pylori* and *Anabaena* apoflavodoxin (44 % identity) has been performed using the COREX algorithm (25). COREX generates, from the tridimensional structure, an ensemble of thousands of different conformations of the protein, from native to totally unfolded, and computes their stabilities (25,26). The parameterization used by COREX predicts well the ΔH(60°C) and ΔS(60°C) values of the global unfolding of *H. pylori* apoflavodoxin at pH 7.0 (104 kcal/mol and 0.31 $kcal.mol^{-1}.K^{-1}$, respectively compared to the experimentally determined values of 107 and 0.33).

The lower unfolding cooperativity of *H. pylori* apoflavodoxin exerts a profound influence in the unfolding equilibrium, which exhibits three significant differences with that of *Anabaena* apoflavodoxin. First, the initial unfolding transition takes place at lower temperatures; second, the last unfolding transition takes place at higher temperatures; and third, cold-denaturation is more pronounced. The local stabilities of the two proteins, as calculated by COREX, explain them all. In Figure 10a, the residue-specific folding constants at 4 °C (solid line) and 65 °C (dotted line) of *H. pylori* (black) and *Anabaena* apoflavodoxins (gray with orange segments) are superimposed. The values of the folding constants at 4 °C in *H. pylori* show a greater dispersion that those of *Anabaena*, which could explain the lower cooperativity of *H. pylori* thermal unfolding. Compared to *Anabaena*, the *H. pylori* protein presents, in average, lower folding constants at 4 °C. In fact, there are two regions with folding constants close to zero. They correspond to a loop involved in the binding of the phosphate moiety of

FMN (residues 9-19) and to residues (129-139) located in the long loop characteristic of long-chain flavodoxins. These two regions have been proposed in *A. vinelandii* apoflavodoxin (42) to unfold independently generating different partially unfolded forms. Besides, the long loop region appears clearly unfolded in the single thermal intermediate of *Anabaena* apoflavodoxin (23). The low stability of these two regions in *H. pylori* suggests that the native state and I_1 are close in the energy landscape, and that the transition between the two may take place at lower temperatures than in *Anabaena* apoflavodoxin. The second distinctive feature of *H. pylori* unfolding, that the last T_m is 10 degrees higher than in *Anabaena*, is also captured by COREX. While *Anabaena* apoflavodoxin appears completely unfolded at 65 °C (all the residues display negative values of Lnk_f at that temperature; Figure 10a), in agreement with the experimental thermal unfolding curves (23), *H. pylori* apoflavodoxin retains some structure at that temperature (T_{m3} = 71 °C at pH 7, Table 1). Finally, the more pronounced cold denaturation experimentally observed (see Figure 6a) is also qualitatively predicted by COREX. The stability of some residues in *H. pylori* apoflavodoxin (specially in the central β-sheet) significantly increases from 4 to 25 °C, which is shown as negative values in the ΔLnk_f plot (black line in Figure 10b). Cold denaturation is not so pronounced in *Anabaena* apoflavodoxin and, accordingly, fewer protein regions display an inversion in their predicted folding constants when the temperature is increased from 4 to 25 °C (gray line in Figure 10b).

The residues involved in FMN binding in *H. pylori* and *Anabaena* flavodoxins are shown in green in Figure 10b, and those known to become unstructured in the *Anabaena* thermal intermediate (that we identify with I_1 in *H. pylori*) are shown in orange. Indeed, there is partial correspondence between the two kinds of regions (see Figure 10b). Inspection of Figure 10b indicates that COREX helps to identify the regions that become unfolded in the thermal intermediate, and those involved in cofactor binding, as the regions displaying large decreases in local stability while the global of the protein keeps invariant, when the temperature is raised from 4 to 25 °C (peaks with positive values of ΔLnk_f in Figure 10b). The overall good correspondence between the regions predicted by COREX to become destabilized as the temperature is raised and those observed to be unstructured in the thermal intermediate (23) is evident in *Anabaena* apoflavodoxin (Figure 10b). In *H. pylori* the correspondence is also clear although some of the putative unstructured regions in I_1 (around residues 60 and 125) experience smaller destabilizations simply because they already present a very low local stability at the lower temperature (see Figure 10a). It is interesting that, although one of the weak regions (around residue 95) does not exhibit low local stability (see Figure 10a), COREX identifies it by its large destabilization at 25 °C relative to 4°C. This work thus suggests that even regions that are predicted to display high local stabilities may get involved in independent unfolding events leading to intermediates, and it seems that analysis of the temperature variation of local stability at temperatures where the native state is the dominant conformation may be useful to identify them.

Acknowledgements

Funding Information: J.S. acknowledges financial support from grants BFU2004-01411 and PM076/2006. N.C. was supported by an FPU fellowship (Spain). A.V.-C. is supported by grant from the Spanish Ministry of Education and Science SAF2004-07722 and is a recipient of a Ramón y Cajal Research Contract from the Spanish Ministry of Science and Technology. E.F. is supported by grants from the National Institutes of Health GM57144 and GM56550 and the National Science Foundation MCB0131241.

References

1. Sancho J. Flavodoxins: sequence, folding, binding, function and beyond. Cell Mol Life Sci 2006;63:855–864. [PubMed: 16465441]

2. Lopez-Llano J, Maldonado S, Bueno M, Lostao A, Angeles-Jimenez M, Lillo MP, Sancho J. The long and short flavodoxins: I. The role of the differentiating loop in apoflavodoxin structure and FMN binding. J Biol Chem 2004;279:47177–47183. [PubMed: 15317816]
3. Lopez-Llano J, Maldonado S, Jain S, Lostao A, Godoy-Ruiz R, Sanchez-Ruiz JM, Cortijo M, Fernandez-Recio J, Sancho J. The long and short flavodoxins: II. The role of the differentiating loop in apoflavodoxin stability and folding mechanism. J Biol Chem 2004;279:47184–47191. [PubMed: 15317817]
4. Rao ST, Shaffie F, Yu C, Satyshur KA, Stockman BJ, Markley JL, Sundarlingam M. Structure of the oxidized long-chain flavodoxin from *Anabaena* 7120 at 2 A resolution. Protein Sci 1992;1:1413–1427. [PubMed: 1303762]
5. Genzor CG, Perales-Alcon A, Sancho J, Romero A. Closure of a tyrosine/tryptophan aromatic gate leads to a compact fold in apo flavodoxin. Nat Struct Biol 1996;3:329–332. [PubMed: 8599758]
6. Genzor CG, Beldarrain A, Gomez-Moreno C, Lopez-Lacomba JL, Cortijo M, Sancho J. Conformational stability of apoflavodoxin. Protein Sci 1996;5:1376–1388. [PubMed: 8819170]
7. Lostao A, El Harrous M, Daoudi F, Romero A, Parody-Morreale A, Sancho J. Dissecting the energetics of the apoflavodoxin-FMN complex. J Biol Chem 2000;275:9518–9526. [PubMed: 10734100]
8. Lostao A, Daoudi F, Irun MP, Ramon A, Fernandez-Cabrera C, Romero A, Sancho J. How FMN binds to *Anabaena* apoflavodoxin: a hydrophobic encounter at an open binding site. J Biol Chem 2003;278:24053–24061. [PubMed: 12682068]
9. Campos LA, Sancho J. Native-specific stabilization of flavodoxin by the FMN cofactor: structural and thermodynamical explanation. Proteins 2006;63:581–594. [PubMed: 16444751]
10. van Mierlo CP, van Dongen WM, Vergeldt F, van Berkel WJ, Steensma E. The equilibrium unfolding of *Azotobacter vinelandii* apoflavodoxin II occurs via a relatively stable folding intermediate. Protein Sci 1998;7:2331–2344. [PubMed: 9827999]
11. Bollen YJ, Nabuurs SM, van Berkel WJ, van Mierlo CP. Last in, first out: the role of cofactor binding in flavodoxin folding. J Biol Chem 2005;280:7836–7844. [PubMed: 15632150]
12. Muralidhara BK, Wittung-Stafshede P. Thermal unfolding of Apo and Holo *Desulfovibrio desulfuricans* flavodoxin: cofactor stabilizes folded and intermediate states. Biochemistry 2004;43:12855–12864. [PubMed: 15461458]
13. Nuallain BO, Mayhew SG. A comparison of the urea-induced unfolding of apoflavodoxin and flavodoxin from *Desulfovibrio vulgaris*. Eur J Biochem 2002;269:212–223. [PubMed: 11784315]
14. Blaser MJ. Hypotheses on the pathogenesis and natural history of *Helicobacter pylori*-induced inflammation. Gastroenterology 1992;102:720–727. [PubMed: 1732141]
15. Parsonnet J, Friedman GD, Vandersteen DP, Chang Y, Vogelman JH, Orentreich N, Sibley RK. *Helicobacter pylori* infection and the risk of gastric carcinoma. N Engl J Med 1991;325:1127–1131. [PubMed: 1891020]
16. Wotherspoon AC, Doglioni C, Diss TC, Pan L, Moschini A, de Boni M, Isaacson PG. Regression of primary low-grade B-cell gastric lymphoma of mucosa-associated lymphoid tissue type after eradication of *Helicobacter pylori*. Lancet 1993;342:575–577. [PubMed: 8102719]
17. Parsonnet J. The incidence of *Helicobacter pylori* infection. Aliment Pharmacol Ther 1995;9:45–51. [PubMed: 8547528]
18. Freigang J, Diederichs K, Schafer KP, Welte W, Paul R. Crystal structure of oxidized flavodoxin, an essential protein in *Helicobacter pylori*. Protein Sci 2002;11:253–261. [PubMed: 11790835]
19. St Maurice M, Cremades N, Croxen MA, Sisson G, Sancho J, Hoffman PS. Flavodoxin:Quinone Reductase (FqrB): a Redox Partner of Pyruvate:Ferredoxin Oxidoreductase That Reversibly Couples Pyruvate Oxidation to NADPH Production in *Helicobacter pylori* and Campylobacter jejuni. J Bacteriol 2007;189:4764–4773. [PubMed: 17468253]
20. Cremades N, Bueno M, Toja M, Sancho J. Towards a new therapeutic target: *Helicobacter pylori* flavodoxin. Biophys Chem 2005;115:267–276. [PubMed: 15752617]
21. Martínez-Júlvez M, Cremades N, Bueno M, Perez-Dorado I, Maya C, Cuesta-Lopez S, Diego P, Falo F, Hermoso JA, Sancho J. Common conformational changes in flavodoxins induced by FMN and anion binding: the structure of *H. pylori* apoflavodoxin. Proteins. 2007In Press

22. Pantoliano MW, Petrella EC, Kwasnoski JD, Lobanov VS, Myslik J, Graf E, Carver T, Asel E, Springer BA, Lane P, Salemme FR. High-density miniaturized thermal shift assays as a general strategy for drug discovery. J Biomol Screen 2001;6:429–440. [PubMed: 11788061]

23. Campos LA, Bueno M, Lopez-Llano J, Jimenez MA, Sancho J. Structure of stable protein folding intermediates by equilibrium phi-analysis: the apoflavodoxin thermal intermediate. J Mol Bio 2004;344:239–255. [PubMed: 15504414]

24. Cremades N, Sancho J, Freire E. The native-state ensemble of proteins provides clues for folding, misfolding and function. Trends Biochem Sci 2006;31:494–496. [PubMed: 16870449]

25. Hilser VJ, Freire E. Structure-based calculation of the equilibrium folding pathway of proteins. Correlation with hydrogen exchange protection factors. J Mol Biol 1996;262:756–772. [PubMed: 8876652]

26. Hilser VJ, Townsend BD, Freire E. Structure-based statistical thermodynamic analysis of T4 lysozyme mutants: structural mapping of cooperative interactions. Biophys Chem 1997;64:69–79. [PubMed: 9127939]

27. Luque I, Freire E. Structural stability of binding sites: consequences for binding affinity and allosteric effects. Proteins Suppl 2000;4:63–71.

28. Edmondson DE, Tollin G. Chemical and physical characterization of the Shethna flavoprotein and apoprotein and kinetics and thermodynamics of flavin analog binding to the apoprotein. Biochemistry 1971;10:124–132. [PubMed: 5538602]

29. Gill SC, von Hippel PH. Calculation of protein extinction coefficients from amino acid sequence data. Anal Biochem 1989;182:319–326. [PubMed: 2610349]

30. Fernando T, Royer CA. Unfolding of trp repressor studied using fluorescence spectroscopic techniques. Biochemistry 1992;31:6683–6691. [PubMed: 1637807]

31. Royer CA, Mann CJ, Matthews CR. Resolution of the fluorescence equilibrium unfolding profile of trp aporepressor using single tryptophan mutants. Protein Sci 1993;2:1844–1852. [PubMed: 8268795]

32. Freire E, Biltonen RL. Thermodynamics of transfer ribonucleic acids: the effect of sodium on the thermal unfolding of yeast tRNAPhe. Biopolymers 1978;17:1257–1272. [PubMed: 247996]

33. Privalov PL, Khechinashvili NN. A thermodynamic approach to the problem of stabilization of globular protein structure: a calorimetric study. J Mol Biol 1974;86:665–684. [PubMed: 4368360]

34. Straume M, Freire E. Two-dimensional differential scanning calorimetry: simultaneous resolution of intrinsic protein structural energetics and ligand binding interactions by global linkage analysis. Anal Biochem 1992;203:259–268. [PubMed: 1416022]

35. Freire E, Biltonen RL. Statistical mechanical deconvolution of thermal transitions in macromolecules. I. Theory and application to homogeneous systems. Biopolymers 1978;17:463–479.

36. Murphy KP, Freire E. Thermodynamics of structural stability and cooperative folding behavior in proteins. Adv Protein Chem 1992;43:313–361. [PubMed: 1442323]

37. Xie D, Freire E. Structure based prediction of protein folding intermediates. J Mol Biol 1994;242:62–80. [PubMed: 8078072]

38. Gomez J, Hilser VJ, Xie D, Freire E. The heat capacity of proteins. Proteins 1995;22:404–412. [PubMed: 7479713]

39. Murphy KP, Bhakuni V, Xie D, Freire E. Molecular basis of co-operativity in protein folding. III. Structural identification of cooperative folding units and folding intermediates. J Mol Biol 1992;227:293–306. [PubMed: 1522594]

40. Zorrilla, S. Máster Thesis Biochemistry Department. Zaragoza University (Spain): Zaragoza; 1998. Departamento de Bioquímica y Biología Molecular.

41. Irun MP, Garcia-Mira MM, Sanchez-Ruiz JM, Sancho J. Native hydrogen bonds in a molten globule: the apoflavodoxin thermal intermediate. J Mol Biol 2001;306:877–888. [PubMed: 11243795]

42. Bollen YJ, Kamphuis MB, van Mierlo CP. The folding energy landscape of apoflavodoxin is rugged: hydrogen exchange reveals nonproductive misfolded intermediates. Proc Natl Acad Sci USA 2006;103:4095–4100. [PubMed: 16537490]

43. Sobolev V, Sorokine A, Prilusky J, Abola EE, Edelman M. Automated analysis of interatomic contacts in proteins. Bioinformatics 1999;15:327–332. [PubMed: 10320401]

44. Campos LA, Garcia-Mira MM, Godoy-Ruiz R, Sanchez-Ruiz JM, Sancho J. Do proteins always benefit from a stability increase? Relevant and residual stabilisation in a three-state protein by charge optimisation. J Mol Biol 2004;344:223–237. [PubMed: 15504413]

45. Rosgen J, Hinz HJ. Phase diagrams: a graphical representation of linkage relations. J Mol Biol 2003;328:255–271. [PubMed: 12684012]

Abbreviations

FMN flavin mono-nucleotide

CD circular dichroism

UV ultraviolet

ITC isothermal titration calorimetry

DSC differential scanning calorimetry

ASA accessible surface area

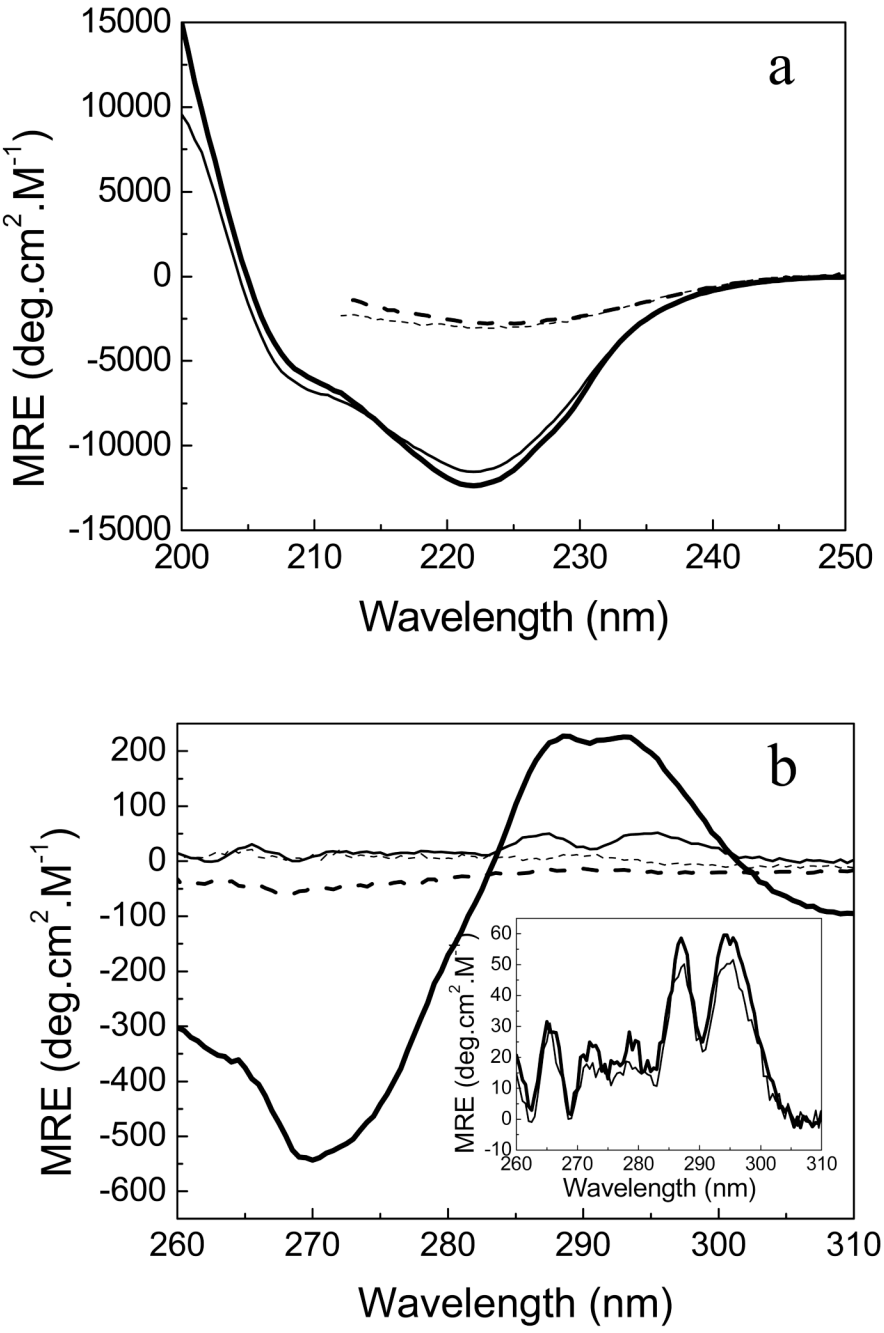

FIGURE 1.

Spectroscopic comparison of *H. pylori* apo (thin lines) and holoflavodoxin (thick lines) in EPPS 50 mM, pH 9.0 under native conditions, at 25°C (continuous lines) and thermally-unfolded at 90 °C (dashed line). Far-UV circular dichroism (a) and near-UV CD (b). The insert in (b) compares the near-UV CD spectrum of apoflavodoxin at pH 9 (thin line) with that at pH 7.0 (thick line). The different spectra of both the apoprotein and holoprotein at pH 7.0 are very similar to the corresponding ones at pH 9.0 (not shown).

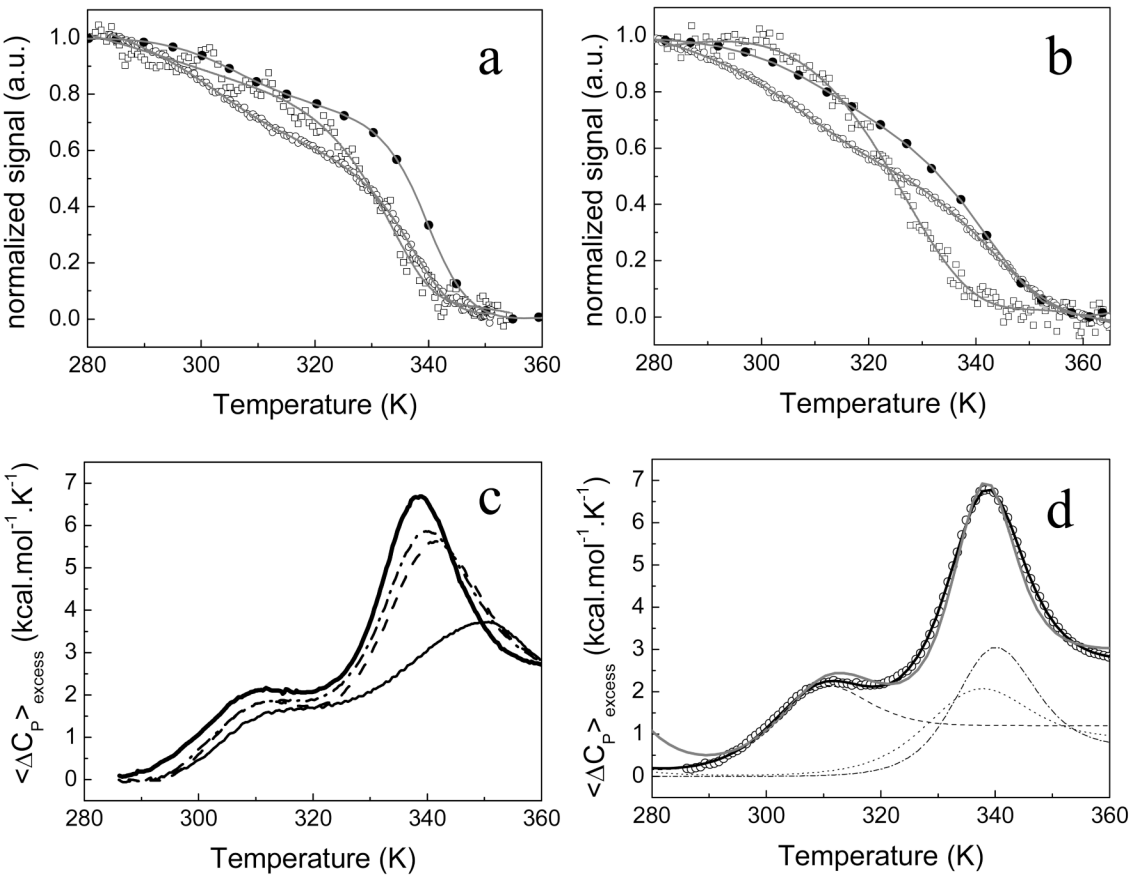

FIGURE 2.

(a) and (b) Thermal denaturation of *H. pylori* apoflavodoxin followed by spectroscopic techniques in EPPS 50mM, pH 9.0 and 50 mM MOPS, pH 7.0, respectively. Fluorescence data is represented as closed circles, far-UV CD as open circles and near-UV CD as open squares. The continuos gray lines represent the best global fit to a four-state model. (c) and (d) DSC of *H. pylori* apoflavodoxin. In figure (c) DSC curves of apoflavodoxin at different pH values: thin continuous line is pH 7.0, dashed line is pH 8.0, dash-dotted line, pH 8.5 and the thick continuous line, pH 9.0. Figure (d) shows the excess heat capacity change at pH 9.0 as a function of temperature. The experimental data (open circles) and the theoretical fit of the data to a three-state model (gray line) and the fit to a four-state model (black line) are shown. The contribution of each transition (the deconvolution) is also represented: the first transition as dash line, the second transition as dotted line and the third one as dash-dotted line.

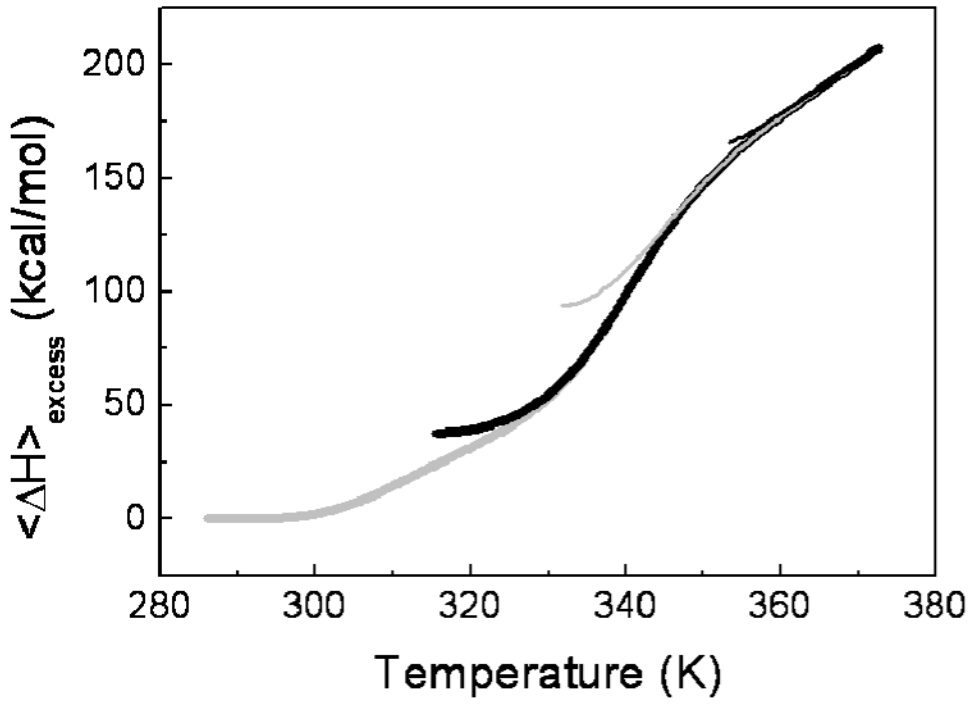

FIGURE 3.

Statistical Mechanical Deconvolution of the thermal denaturation of *H. pylori* apoflavodoxin in EPPS 50 mM pH 9.0, followed by differential scanning calorimetry. The grey thick line represents the enthalpy function obtained directly from the integration of the calorimetric experiment. The black thick line represents the excess enthalpy change after the contribution of the first transition is eliminated. The grey and black thin lines correspond to the excess enthalpy change after removing the contribution of the subsequent macroscopic states using the recursive method (see Materials and Methods), i.e., the first intermediate and the second intermediate, respectively.

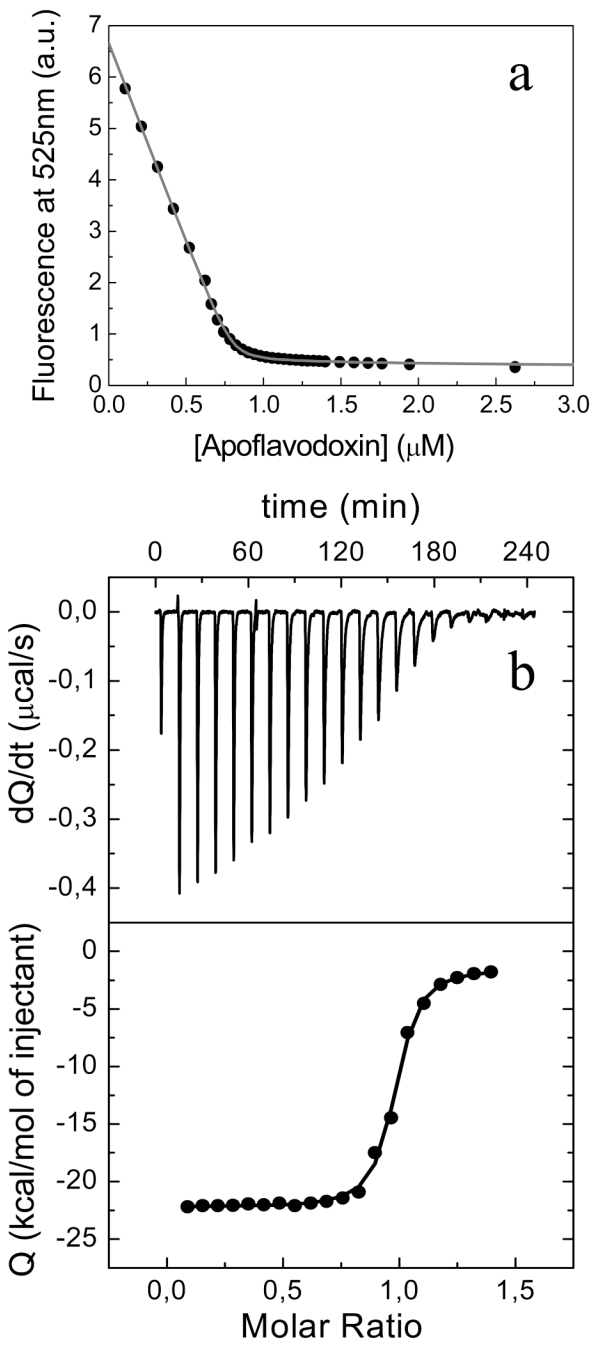

FIGURE 4.

FMN binding to *H. pylori* flavodoxin. (a) Titration of FMN binding at 25 °C in MOPS 50 mM, pH 7.0 by fluorescence quenching at 525nm. The experimental data is represented by filled circles and its fit by a gray line. (b) ITC experiment in the same conditions as in (a). Due to kinetic effects upon FMN binding in the last part of the titration, the time between injections was increased to 700 s.

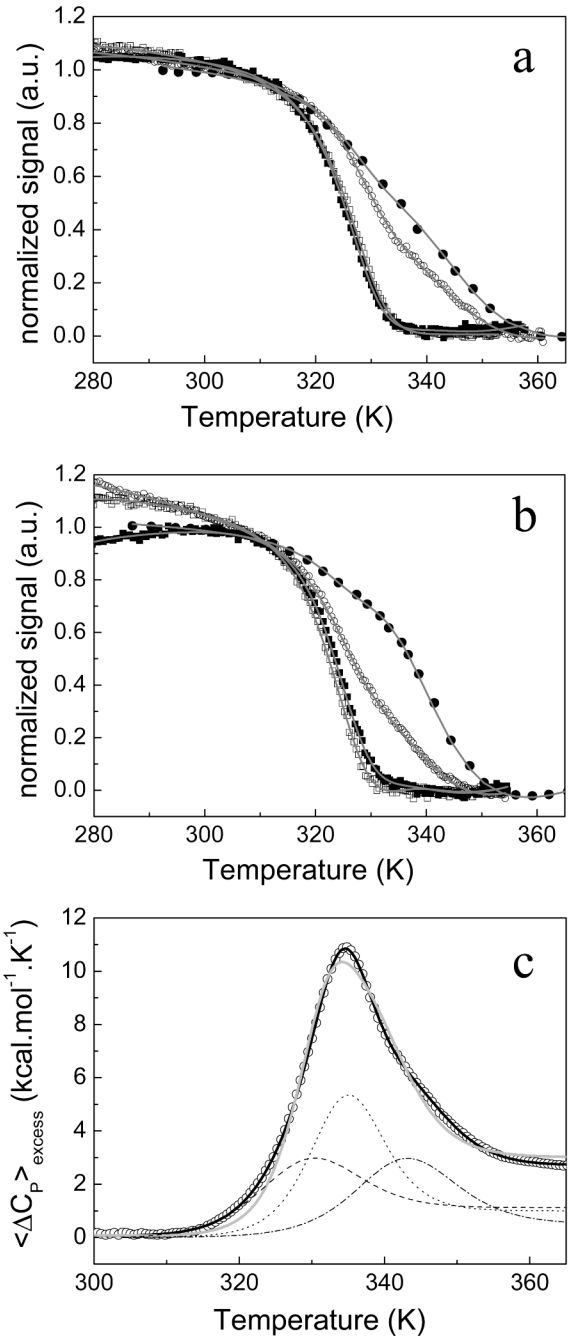

FIGURE 5.

Thermal denaturation of flavodoxin followed spectroscopically in 50 mM MOPS, pH 7.0 (a) and EPPS 50mM, pH 9.0 (b). Fluorescence data is represented as closed circles, far-UV CD as open circles, near-UV CD as open squares and visible CD as closed squares. The continuous gray lines represent the best global fit to a four-state sequential unfolding model. A DSC experiment of holoflavodoxin in EPPS 50mM, pH 9.0 is shown as open circles in (c). The gray line correspond to the theoretical fit of the experimental data to a three-state model and the black line, the fit to a four-state model. The contribution of each of the three transitions are also represented as dashed, dotted and dash-dotted lines.

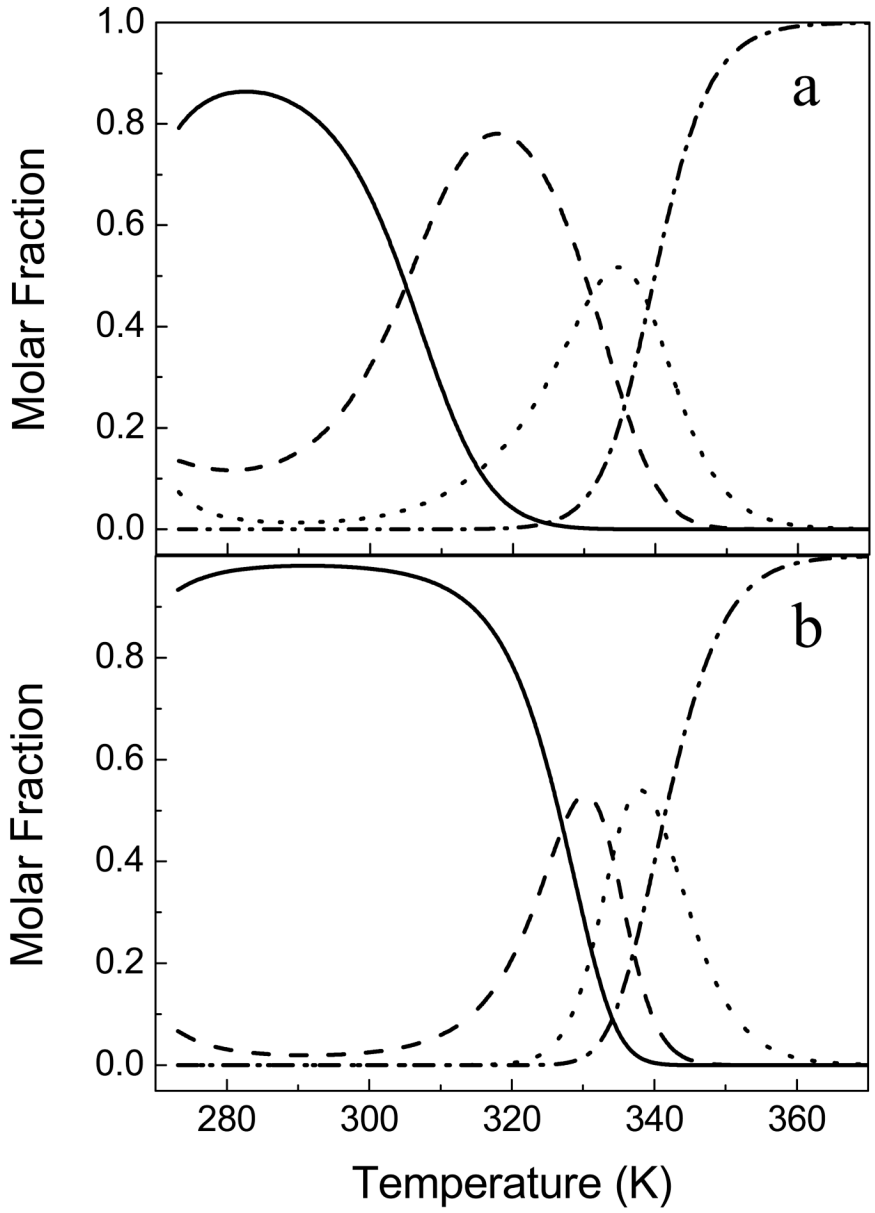

FIGURE 6.

Temperature dependence, at pH 9.0, of the four macroscopic states of *H. pylori* apoflavodoxin (a) and holoflavodoxin (b): native (continuous line), first thermal intermediate, I_1 (dashed line), the second intermediate, I_2 (dotted line) and the unfolded state (dash-dotted line). The thermodynamic parameters used to calculated the molar fractions of the different states were the ones obtained from DSC analysis (Table 1 and 3). The sequential unfolding model was used both to fit and to calculate the molar fractions.

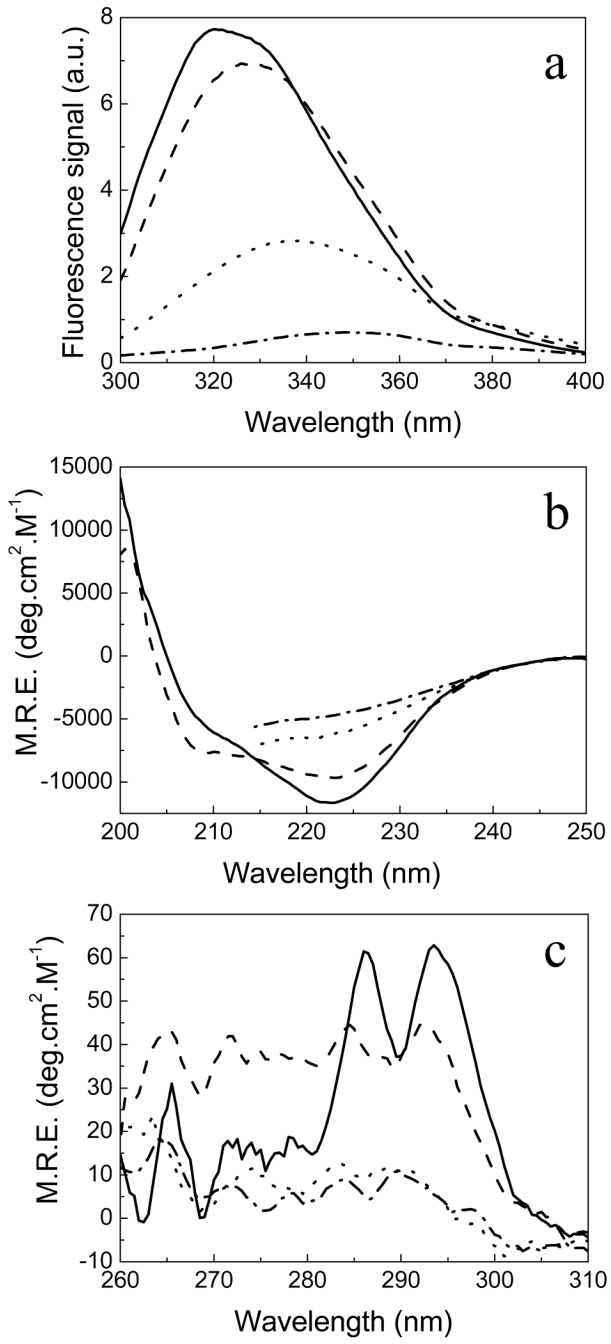

FIGURE 7.

Spectroscopic characterization of the four significantly populated states of *H. pylori* apoflavodoxin (sequential thermal unfolding model) by spectra deconvolution: native (continuous line), first thermal intermediate, I_1 (dashed line), the second intermediate, I_2 (dotted line) and the unfolded state (dash-dotted line). Fluorescence (a), far-UV CD (b), and near-UV CD (c) spectra.

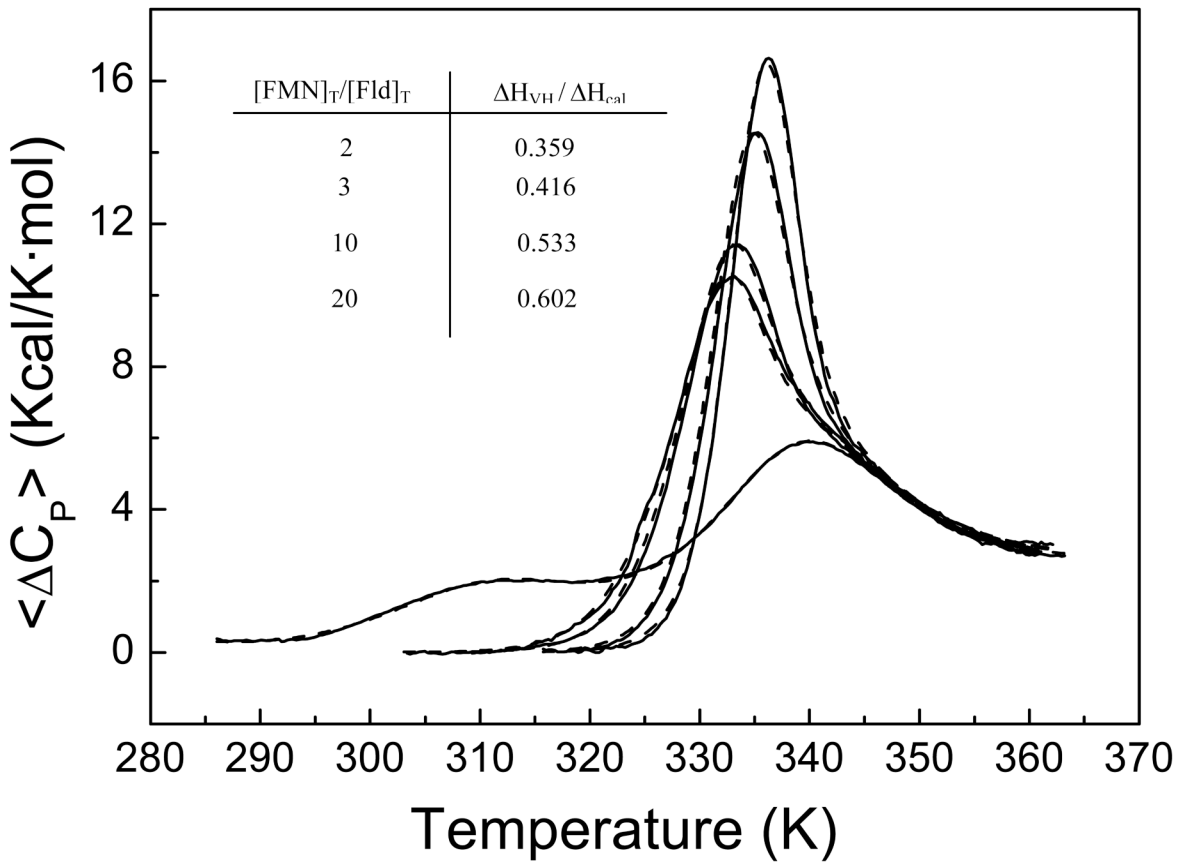

FIGURE 8.

Thermal unfolding of *H. pylori* flavodoxin at five different total concentrations of FMN: 0, 32.6, 48.9, 163 and 326 μM. The concentration of protein is 16.3 μM. The experiments were made in Tris 165 mM, pH 8.5. In the absence of ligand, the protein exhibits three transitions (the endothermic peak at high temperature is not a single unfolding transition, but the superposition of two close transitions). The transition most affected by the FMN binding is the one taking place at low temperature.

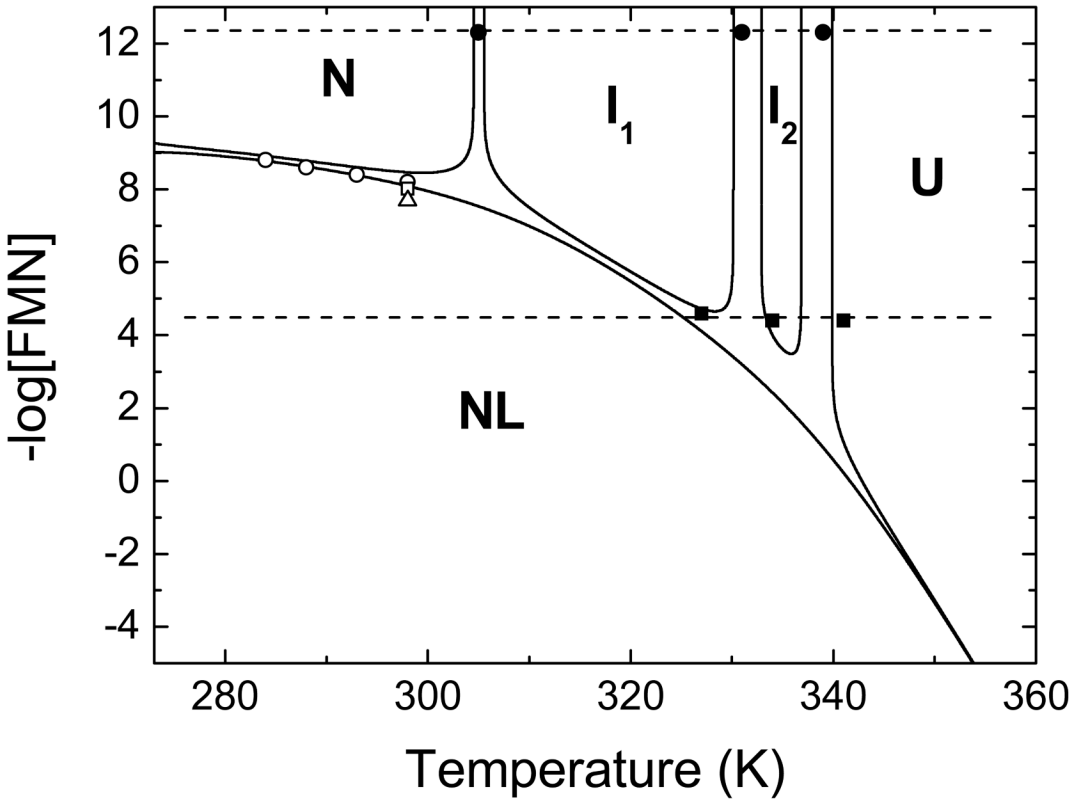

FIGURE 9.

Temperature-ligand concentration phase diagram for the coupling of the conformational equilibrium and the binding equilibrium in the flavodoxin-FMN system at pH 9.0. Continuous lines, engulfing regions where the specified conformation is dominant, are constructed as the geometric sites of the points at which a given species populates 50% of the total protein concentration, using the parameters determined for unfolding and binding at pH 9.0. The different species are represented by: N (native unliganded), NL (native liganded), I_1 (first intermediate), I_2 (second intermediate), and U (unfolded protein). The two dotted lines represent trajectories of typical temperature denaturations in the absence (top) and the presence (bottom) of FMN. Experimentally determined parameters are indicated with symbols: binding affinity estimated by spectroscopy (open circles), DSC (open square), and ITC (open triangle); unfolding transition temperatures in the absence (closed circles) and presence of FMN cofactor (closed squares).

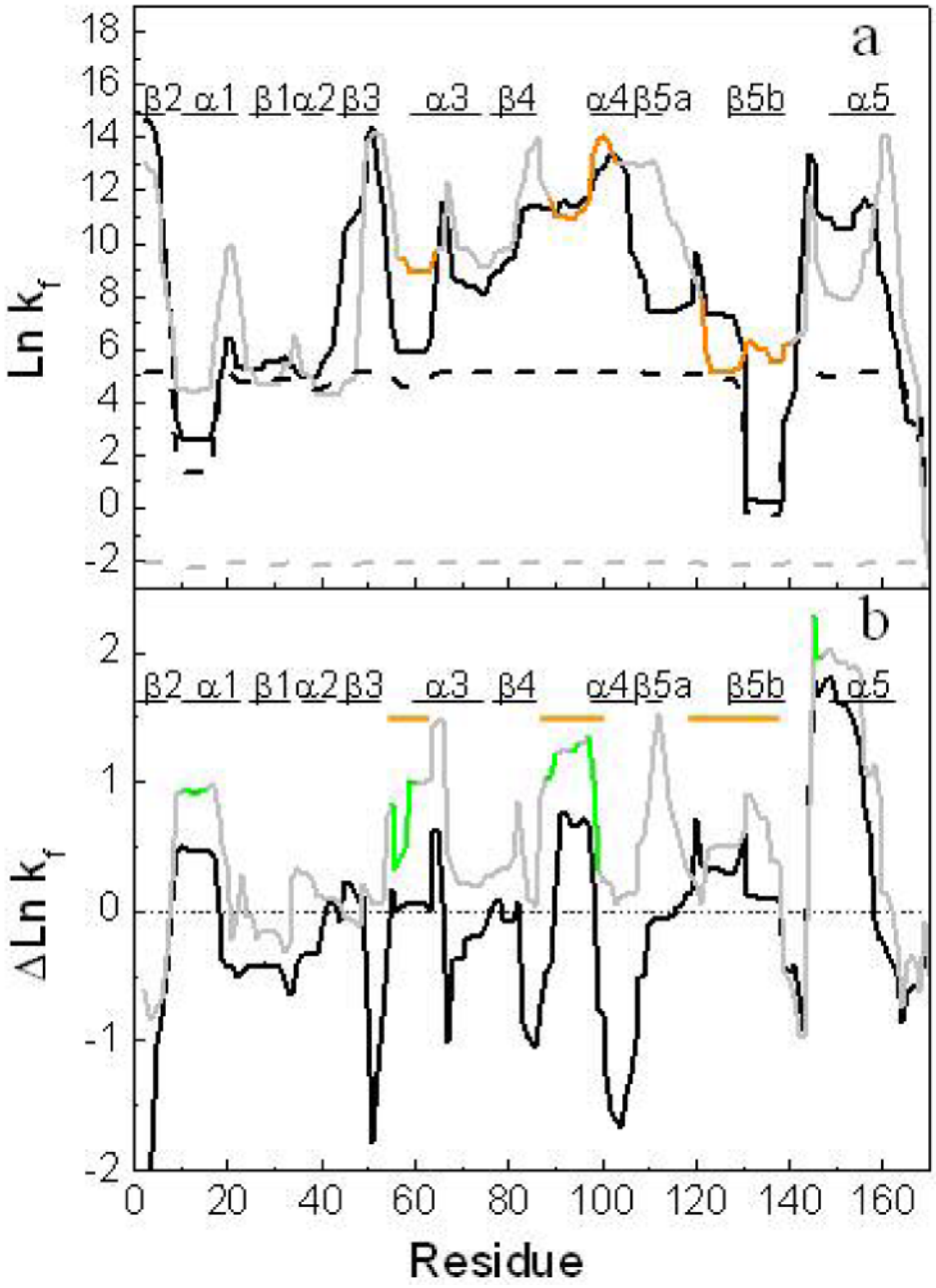

FIGURE 10.

Local stability of *H. pylori* apoflavodoxin compared to that of *Anabaena* apoflavodoxin. (a) Natural logarithms of the predicted folding constant with COREX algorithm (ln k_f) for each amino acid of *H. pylori* apoflavodoxin at 4 °C (black line) and *Anabaena* apoflavodoxin (gray line) and at 65 °C (in dashed line). The regions determined to be unfolded by equilibrium Φ-analysis(23) in the thermal intermediate of *Anabaena* apoflavodoxin are colored in orange. The elements of secondary structure of the proteins are shown at the top. (b) Difference in folding constant values of *H. pylori* (black line) and *Anabaena* (gray line) between 4 °C and 25 °C. The FMN binding regions in *Anabaena* flavodoxin are colored in green, the proposed unfolded regions in the thermal intermediate are marked as orange lines. For a better comparison between proteins and its structural elements, a sequence alignment was performed

and the predicted folding constant per residue were plotted in the resulted sequences in both figures.

Table 1

Stability of *H. pylori* apoflavodoxin towards thermal unfolding[a]

Three-state analysis	**1st Transition**		**2nd Transition**	
	T_{m1}	ΔH_1	T_{m2}	ΔH_2
DSC_{vH}	305 ± 2	29 ± 3	337.6[b]	50
Fluorescence	307 ± 1	26 ± 2	339.2 ± 0.3	52 ± 1
Far-UV CD	306 ± 5	27 ± 4	337.2 ± 0.6	44 ± 3
Near-UV CD[c]	305	26	333[d]	36

Four-state analysis	**1st Transition**			**2nd Transition**			**3rd Transition**		
	T_{m1}	ΔH_1	ΔC_{P1}	T_{m2}	ΔH_2	ΔC_{P2}	T_{m3}	ΔH_3	ΔC_{P3}
DSC_{cal} pH 9	305 ± 2	29 ± 3	1.2 + 0.2	331 ± 2	33 ± 2	1.01 ± 0.07	339.1 ± 0.2	52 ± 2	0.48 ± 0.05
Spectr. pH 9[e]	305 ± 2	29 ± 3		333 ± 4	30 ± 8		340 ± 2	59 ± 5	
Spectr. pH 7[e]	307 ± 3	21 ± 3		331 ± 2	26 ± 3		344 ± 5	34 ± 9	

[a] In EPPS 50 mM, pH 9.0, unless otherwise indicated. The units are: T_m (K), ΔH (kcal.mol^{-1}) and ΔC_P (kcal.mol^{-1}.K^{-1})

[b] This T_m is the temperature of the top of the second peak, ΔH corresponds to the van't Hoff enthalpy of the peak.

[c] Due to the high level of noise obtained with this technique, the fitting errors are very large (not show).

[d] This value is inferred from a superposition of the near CD curves at pH 7.0 y 9.0.

[e] Parameters obtained from global fit of all the spectroscopic curves to equation 1.

Table 2

Apoflavodoxin/FMN binding energetics

Parameter	Protein			
	H. pylori[a]		*Anabaena* WT[b]	*Anabaena* W57A[c]
	pH 7	pH 9	pH 7	pH 7
ITC				
K_d (nM)	27 ± 1	23 ± 2	-	-
ΔG (kcal/mol)	-10.3 ± 0.1	-10.3 ± 0.1	-	-
ΔH (kcal/mol)	-21 ± 0.3	-25 ± 0.2	-11.8 ± 0.3	-7.1 ± 0.2
ΔS (cal.mol^{-1}.K^{-1})	-36 ± 1	-49 ± 0.7	-	-
ΔC_P (cal.mol^{-1}.K^{-1})	-600 ± 30[d]	-	-600 ± 20	-620 ± 50
Spectroscopy				
K_d (nM)	4.4 ± 0.7	-	0.26 ± 0.06	5.2 ± 0.9 (11.4)
ΔG (kcal/mol)	-11.4 ± 0.5	-	-13.1 ± 0.1	-11.3 ± 0.1 (-10.8)
ΔH[e] (kcal/mol)	-14 ± 2	-	-	-
ΔS (cal.mol^{-1}.K^{-1})	-7.7 ± 6	-	8 ± 2[f]	14 ± 1[f]

[a] At 25 °C, in MOPS 50 mM, pH 7.0 or EPPS 50 mM, pH 9.0. The errors reported in this Table were provided by the fitting program and propagated when required.

[b] At 25 °C in MOPS 50 mM, pH 7.0(ref. 7). ΔH and ΔS values were measured in 50 mM phosphate, pH 7.0.

[c] At 25 °C in 50 mM phosphate, pH 7.0 (ref. 7). Values in parenthesis were obtained in 50 mM MOPS, pH 7.0.

[d] Calculated as the slope of ΔH vs T at 10, 15, 20 and 25 °C.

[e] Calculated from spectroscopic titrations at 11, 15 and 20 °C (K_d = 2.1, 3.4 and 4.4 nM, respectively).

[f] ΔS in this case was calculated from the ΔG value spectroscopically determined and the calorimetrically measured ΔH value.

Table 3

Stability of *H. pylori* holoflavodoxin towards thermal unfolding[a]

Three-state analysis	**1st Transition**		**2nd Transition**	
	T_{m1}	ΔH_1	T_{m2}	ΔH_2
DSC_{vH}	335	58		
Fluorescence	324 ± 1	30 ± 2	341 ± 1	50 ± 2
Far-UV CD	324 ± 0.5	55 ± 1	337 ± 1	65 ± 5
Near-UV CD[c]	323.2 ± 0.1	63 ± 1		
Visible CD	323.7 ± 0.1	54 ± 1		

Four-state analysis	**1st Transition**			**2nd Transition**			**3rd Transition**		
	T_{m1}	ΔH_1	ΔC_{P1}	T_{m2}	ΔH_2	ΔC_{P2}	T_{m3}	ΔH_3	ΔC_{P3}
DSC_{cal} pH 9	327.2 ± 0.2	43 ± 0.5	1.2	334 ± 1	65 ± 1	1.0	341 ± 0.5	50 ± 1	0.5
Spectr. pH 9[b]	325.1 ± 0.5	44 ± 1		331 ± 1	51 ± 4		341 ± 1	40 ± 2	
Spectr. pH 7[b]	327 ± 3	43 ± 10		335 ± 5	32 ± 10		344 ± 5	43 ± 10	

[a] In EPPS 50 mM, pH 9, unless otherwise indicated. Units: T_m(K), ΔH (kcal.mol^{-1}), ΔC_P (kcal.mol^{-1}.K^{-1})

[b] Parameters obtained from the global fit to equation 1.